Control System Design in the Presence of Severe Structural Dynamics Interactions

John F. Yocum* and Loren I. Slafer†
Hughes Aircraft Company, El Segundo, Calif.

Control system design in the presence of severe structural/control loop interactions is treated by presenting the case history of the Orbiting Solar Observatory-8 despin control loop. Analytical design work, subsequent ground testing, and resulting in-orbit behavior are discussed. The analytical work, which is based upon the hybrid coordinate method of structural dynamic modeling, led to electronic compensation of some structural modes. Ground tests of the structure, conducted to verify analytical predictions, resulted in further modifications of the design.

I. Introduction

THE influence of flexible body dynamics on spacecraft attitude control is becoming increasingly significant as vehicle configurations become more unwieldy and control requirements become more demanding. Incorporation of large, flexible solar panels or steerable payloads in configurations of newer spacecraft (such as CTS, MARINER-4, DSCS III, INTELSAT V, and TDRS), and the development of precision pointing optical instruments to fly on future spacecraft have led to complex control problems involving spacecraft structural dynamics. Future requirements of the very large space structures being considered (such as the Space Station, Solar Power Station, and Solar Sail) pose even more demanding design problems.

In coming to grips with these problems, several spacecraft designers have developed general purpose computer programs for simulation and/or analysis of flexible controlled spacecraft.[1-3] These programs accomplish time simulation as well as control loop stability analysis and design for flexible space vehicles. This paper describes the experience gained with the first generation of such programs developed during the Orbiting Solar Observatory (OSO)-8 project and successfully applied to several other projects. The basic analysis technique, as described in Sec. III, utilizes modal models of flexible elements and employs frequency domain analysis to evaluate the stability of the control loop/flexible dynamics coupling. Bode plots, along with plots of open-loop system gain vs phase (Nichols graphs), are used extensively to provide both quantitative and qualitative descriptions of the coupling dynamics.

Testing of the flexible spacecraft to verify stability of the control/structural interaction can become a major item in many programs. Traditionally, modal surveys have been relied upon as the major tool in verifying that the flexible spacecraft behaves as predicted by detailed structural analysis. This is an expensive, time-consuming test and yields a very indirect measure of control loop stability or performance margins. On OSO-8, classical open-loop frequency response measurements were combined with a loop shaping perturbation technique to obtain a direct measure of stability margins and closed-loop damping associated with principal flexible modes.

Received July 13, 1977; revision received Oct. 25, 1977.

Index categories: Spacecraft Dynamics and Control; Spacecraft Testing, Flight and Ground; Structural Dynamics.

*Senior Staff Engineer, Guidance and Control Systems Laboratory, Space and Communications Group.

†Senior Staff Engineer, Guidance and Control Systems Laboratory, Space and Communications Group. Member AIAA.

This paper describes the analysis and test techniques developed and presents results of these techniques as applied to the OSO-8 spacecraft. Limited flight data from the OSO spacecraft are also discussed.

II. OSO Vehicle and Mission Requirements

Attitude control hardward items for the dual spin OSO-8 spacecraft are illustrated in Fig. 1. The despun platform is comprised primarily of a solar panel and the pointed instrument assembly (PIA). The two independent experiment packages making up the PIA rely on solar-oriented telescopes (spectrometers) to collect scientific data concerning variation of the ultraviolet lines on the solar disk, particularly in the chromosphere. Additional scientific experiments are contained within the spinning rotor.

The PIA has two degrees of rotational freedom to permit solar pointing. Azimuth motion is achieved by rotating the entire despun platform about the despin bearing axis (DBA), while elevation motion of the PIA alone is facilitated by an elevation bearing assembly (EBA). Both bearing assemblies house electric torque motors used for control. Two sets of attitude sensors are provided. For eclipse periods (once per 90-min orbit), a rate integrating gyro and a microsyn gimbal angle sensor detect azimuth inertial angle and elevation gimbal angle. The primary sun sensors for use when the sun is visible (day) are located on the front faces of the PIA experiment packages, one sensor on each experiment. By viewing a light beam through the experiment telescope optics as well as the sun's direct light, these sensors provide a high-accuracy analog signal proportional to the angular error between the telescope optical axis and the line of sight (LOS) to the sun.

Low-bandwidth servo loops hold attitude during the eclipse periods. At sunrise, control is automatically transferred to

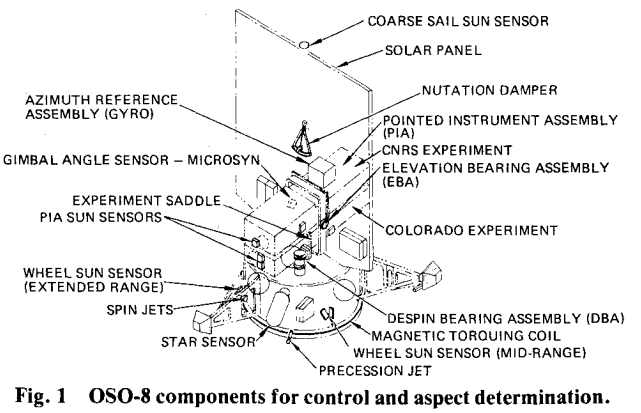

Fig. 1 OSO-8 components for control and aspect determination.

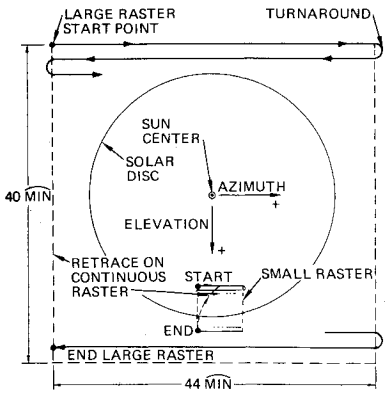

Fig. 2 Control system pointing and raster scan parameters.

RASTER SPECIFICATIONS		
SPECIFICATION	LARGE RASTER	SMALL RASTER
RASTER SIZE (ELEV X AZIMUTH IN ARCMINUTES)	40 X 44	2.5 X 2.75
NO. OF SCAN LINES PER RASTER	64 OR 128	8 OR 16
LINE PERIODS AVAILABLE, SECONDS	20.48 OR 5.12	20.48 OR 5.12
ALLOWABLE TURNAROUND TIME, SECONDS	3.07 OR 0.77	3.07 OR 0.77

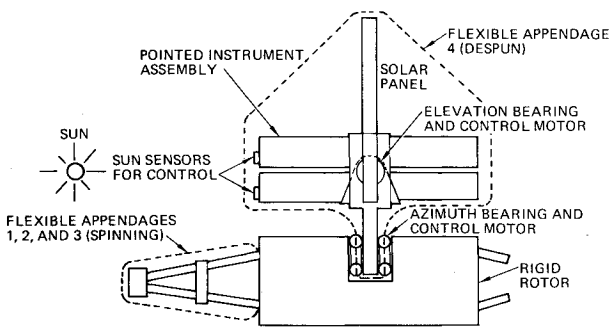

Fig. 3 Breakdown of OSO-8 into rigid body and flexible appendages.

high-bandwidth "day" servos. In addition to highly stable sun center and offset pointing, these servos provide for a fine and coarse "box"-type (raster) scan capability (shown in Fig. 2). The despun platform is scanned back and forth in azimuth while the PIA is repetitively stepped in elevation. This creates a raster which may cover the entire sun (large raster) or a 150- by 150-arc-s portion (small raster) located arbitrarily on the sun's disk. The 1-arc-s pointing stability is maintained throughout, except during the raster scan turnarounds.

III. Structural Dynamics Modeling

The hybrid coordinate modeling approach of Likins[4] was used to develop linearized differential equations of motion for spacecraft dynamics. As depicted in Fig. 3, the spacecraft is modeled as a rigid rotor with four flexible appendages: three ballast booms plus the despun platform. Discrete mass/spring structural models were developed for each appendage. Equations were linearized about a zero platform rate and constant rotor spin rate (6 rpm). Modal analyses of the linearized equations for each appendage were conducted using a modal analysis program which operated on the equations of the form $M\ddot{q}+Kq=$ forcing terms, where M is diagonal and K is symmetric. Other terms in the linearized equation, including skew symmetric rate terms arising from gyroscopic forces, and off-diagonal acceleration terms arising from translational accelerations of the rotor center of mass, were transposed to the right-hand side of the equation and carried along as forcing terms. The final linearized equations are obtained after truncation of higher-frequency modes and application of the usual modal transformations. The resulting equations, although linear, are time varying, as certain terms involving the flexible boom modal variables contain coefficients depending upon the periodic coordinate transformation matrix relating platform and wheel coordinate frames. Laplace transform analyses cannot be applied unless the time varying terms are altered or eliminated. If one assumes that the three booms have identical mode shapes and frequencies, a transformation of variables exists which will eliminate the time-dependent coefficients. This was not pursued, as one primary concern in connection with the boom dynamics was the possible effect of beating between similar modes of slightly unequal frequencies. This question was dealt with through an analog computer simulation of the entire set of equations, together with the control equations. Simulation studies included exercising the control servos in all modes, as well as parametric runs to examine possible beating effects. Results showed that boom modes were indeed excited somewhat by PIA rastering. However, boom dynamics could not be discerned in the servo error signals and no instabilities could be created. As a result of these studies, flexible boom dynamics were excluded from PIA servo stability analyses. The booms were, in effect, assumed rigid, and associated terms were dropped from the mathematical model.

The discrete mass model for the despun platform included 69 mass elements. These were largely mass points having only translational inertia, although rotational inertia was assigned to those points at which control torques were to be exerted. Boundary conditions for the modal analysis clamped the despun platform base in translation and in its transverse rotational axes. The despin and elevation bearing axes were free to rotate, resulting in two zero-frequency, rigid body modes. Twenty (18 flexible and 2 rigid body) modes were retained after modal truncation. Figure 4 illustrates the six most significant mode shapes and frequencies.

An analytic expression for the spacecraft dynamics transfer function matrix is derived from the time invariant linear differential equations. If, in addition to the rigid booms, one assumes a symmetric rotor, the equations take the form

Rigid Body

$$I\ddot{\theta}+H\dot{\theta}-D^T\ddot{\eta}=B_R u \tag{1}$$

Flexible Sail

$$I_F\ddot{\eta}+2Z\Omega\dot{\eta}+\Omega^2\eta-D\ddot{\theta}=B_F u \tag{2}$$

Sensor Output

$$y=C_R\theta+C_F\eta \tag{3}$$

The subscripts R and F refer to rigid and flexible body terms. In particular, the flexible body coefficients B_F, C_F, I_F, and D all depend upon the platform mode shapes. The diagonal structural damping matrix Z contains arbitrarily guessed modal damping ratios. Although various damping ratios were examined in a sensitivity study, a value of 0.005 was used as a baseline. By taking Laplace transforms (with zero initial conditions) of Eqs. (1-3), solving Eq. (2) for $\eta(s)$, substituting this into Eq. (1), and solving for $\theta(s)$, then plugging these results into Eq. (3), one obtains an expression for the 2×2 transfer function matrix relating azimuth and elevation sensor outputs $Y(s)$ to the azimuth and elevation control torque inputs $U(s)$. The result, given in Fig. 5, is still in terms of various matrix functions of s, including some inverses. Although it is possible to expand these expressions analytically and obtain the transfer functions as ratios of polynomials in s, this represents a Herculean effort which is unnecessary. In the analysis that follows, the transfer functions in Fig. 5 were evaluated numerically whenever needed by

simply substituting $s=j\omega$ and evaluating the expressions using computer complex number arithmetic.

Figure 6 shows the data flow and sequence of digital computer programs to accomplish the necessary number crunching. The modal analysis programs (MARS and COMOSY) have existed for some time and have been used primarily by the structural mechanics group to study launch loads. The latter three programs, FLEDCO, NICHOLS 1, and NICHOLS 2, were developed during the OSO-8 program. The NICHOLS 1 program computes the $m \times r$ complex matrix transfer functions of the flexible spacecraft dynamics and stores it on tape for later use by NICHOLS 2. This is cost effective, since generation of the original matrix transfer function is time consuming.

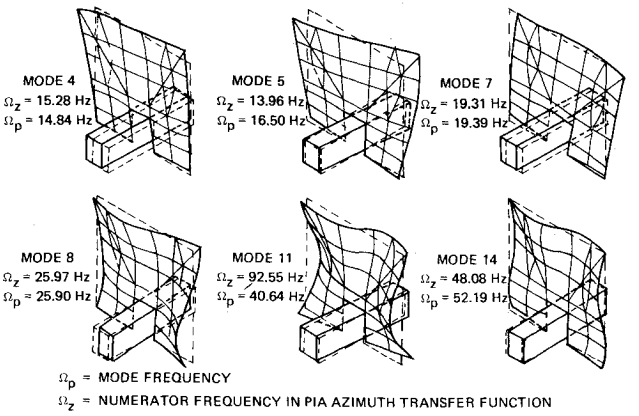

Fig. 4 Shapes of predominant azimuth coupled flexible modes.

EOS OF MOTION:

RIGID BODY $I\ddot{\underline{\theta}} + H\dot{\underline{\theta}} - D^T\ddot{\underline{\eta}} = B_R\underline{u}$ — n EOS (n = 3 FOR OSO); r CONTROL ELEMENTS (r = 2 FOR OSO)

FLEXIBLE BODY $I_p\ddot{\underline{\eta}} + 2Z\Omega\dot{\underline{\eta}} + \Omega^2\underline{\eta} = D\ddot{\underline{\theta}} + B_F\underline{u}$ — p EOS (p = 20 FOR OSO)

OUTPUT RELATION $\underline{y} = C_R\underline{\theta} + C_F\underline{\eta}$ — m EOS (m = 2 FOR OSO)

TAKE LAPLACE TRANSFORMS, SOLVE FOR Y(S)

$$\underline{Y(S)} = \frac{1}{S^2}\left[C_R \mid C_F\right]\left[\begin{array}{c|c} J^{-1}(S) & J^{-1}(S)D^T G^{-1}(S) \\ \hline G^{-1}(S)DJ^{-1}(S) & \left(G^{-1}(S)D\,J^{-1}(S)D^T + E_p\right)G^{-1}(S) \end{array}\right]\left[\begin{array}{c} B_R \\ \hline B_F \end{array}\right]\underline{U(S)}$$

$G(S) = I_p + 2Z\Omega/S + \Omega^2/S^2$

$J(S) = I\text{-}D^T G^{-1}(S)D + H/S$

$I_p = E_p - B_c B_c^T \frac{I}{M_T}$

Fig. 5 Transfer function analysis.

IV. PIA Servo Compensation Design

Although both the elevation and azimuth servo loops experienced significant flexible dynamic coupling, the azimuth loop problems were most severe and attention is focused on that loop. The design rationale followed a three-step process:

1) With the spacecraft dynamics treated as rigid, establish the loop bandwidth and rigid body compensation required to meet pointing accuracy and raster turnaround requirements.

2) Incorporate flexible dynamic model and modify, if necessary, the servo compensation to stabilize flexible modes.

3) Use ground tests to verify structural dynamic model and loop stability. Alter loop compensation if required.

Step 1 employed observer theory to establish an acceptable rigid body design based on pointing jitter and raster turnaround requirements. Step 2 was an iterative exercise in shaping of the open-loop transfer function. Figure 7 shows a block diagram of the design which emerged. The compensation filter includes a flexible dynamics compensation stage as well as a rigid body stage. The parallel integrator path at the compensation output serves to estimate and bias out the average bearing friction torque. Its low gain and limited input and output prevent it from interfering with the transient response during rastering. Figures 8 and 9 illustrate the open-loop bode and gain-phase plots used for stability analysis, and show the characteristics of the modal coupling prior to and following the addition of flexible mode compensation to the servo. The structural dynamics model for this analysis includes 20 modes, although some of these do not couple into azimuth, and their effect is not visible on the plots. The structural dynamics transfer function has the general form

$$G(s) = \frac{1}{Is^2}\prod_{i=1}^{P}\left\{\frac{(s^2/\Omega_{zi}^2) + 2\zeta_i(s/\Omega_{zi}) + 1}{(s^2/\Omega_{pi}^2) + 2\zeta_i(s/\Omega_{zi}) + 1}\right\}$$

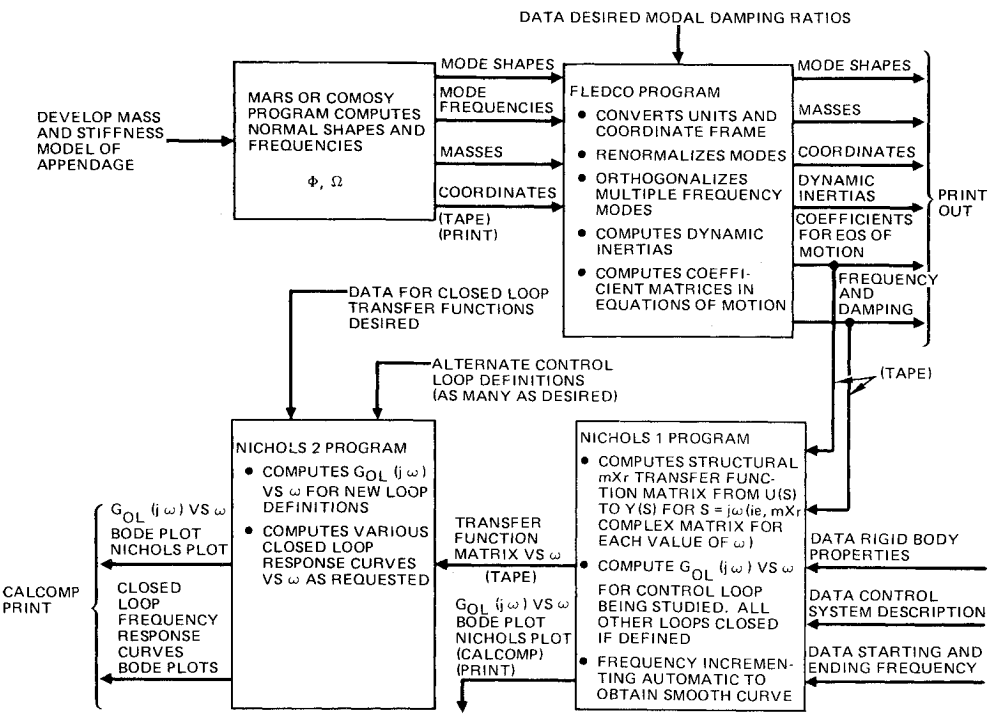

Fig. 6 Control loop analysis data flow.

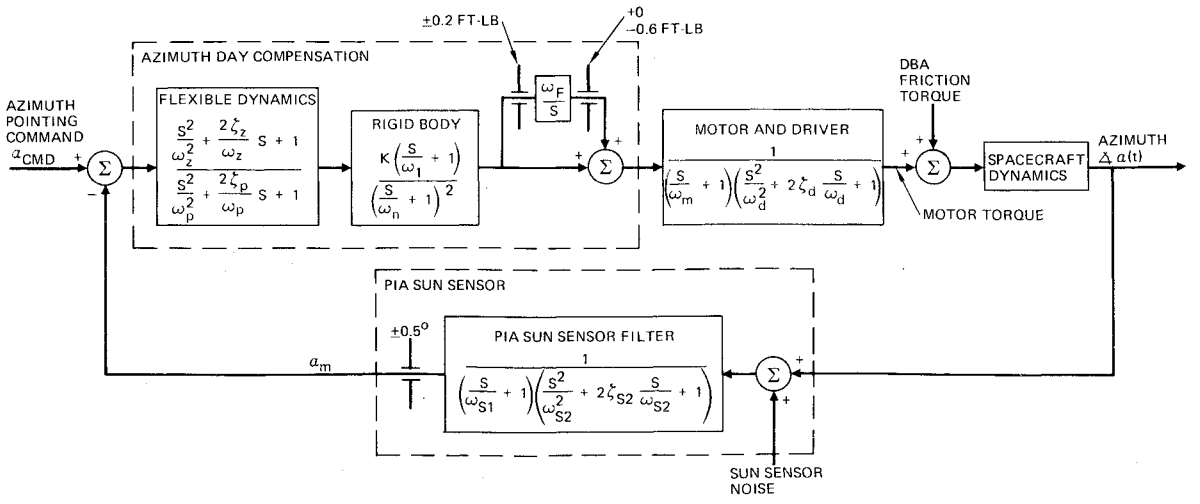

DYNAMICS		COMPENSATION	
SENSOR	MOTOR AND DRIVER	FLEXIBLE DYNAMICS	RIGID BODY
ω_{S1} = 668 rad/sec	ω_m = 17970 rad/sec	ω_z = 80 rad/sec	K = 85 ft-lb/deg
ω_{S2} = 621 rad/sec	ω_d = 1508 rad/sec	ζ_z = 0.3	ω_1 = 8.33 rad/sec
ζ_2 = 0.537	ζ_d = 0.9	ω_p = 160 rad/sec	ω_n = 80 rad/sec
		ζ_p = 0.6	ω_f = 1 rad/sec

Fig. 7 Azimuth day servo loop.

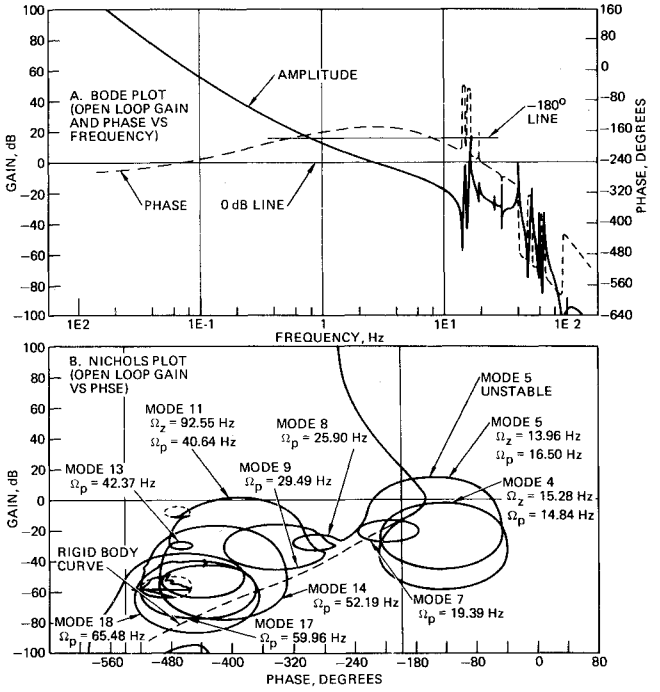

Fig. 8 Stability analysis of azimuth day loop design prior to flexible dynamic compensation.

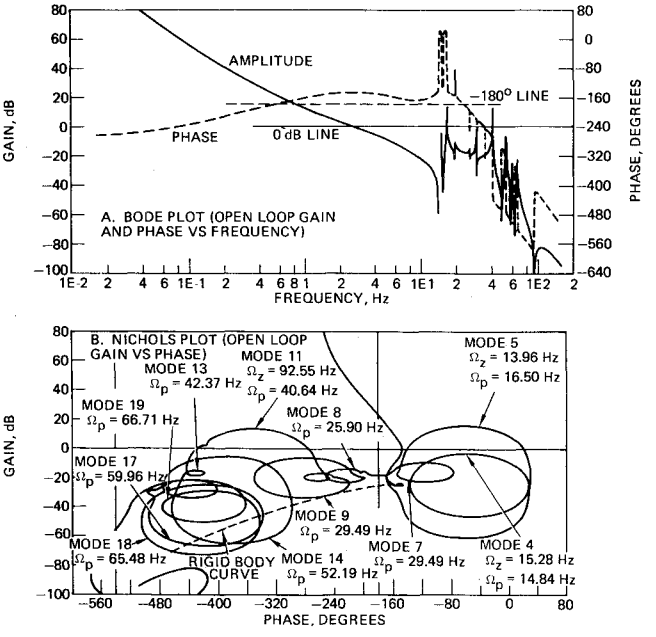

Fig. 9 Stability analysis of azimuth day loop design with flexible dynamic compensation.

where p = number of modes retained in truncated model and values of Ω_{zi} and Ω_{pi} for each mode are indicated on Fig. 8b. Damping ratios of 0.005 were used for all modes. In general, each mode affects the gain-phase plot by contributing a counterclockwise loop to the basic rigid body dynamics curve (shown lightly dashed in Fig. 9b). Note that Modes 5 and 11 exhibit the strongest coupling with the servo loop, as evidenced by peak amplitudes on the Bode or gain-phase plots. Mode 14 is also strongly coupled, but its frequency is sufficiently high that the loop attenuation precludes any stability problems.

The concepts of phase stable and gain stable modes are useful in evaluating loop stability and sensitivity to modeling errors. Very briefly, they are as follows:

1) A phase stabilized mode is one which, for arbitrarily small structural damping ratio, is closed-loop stable regardless of how high the loop gain is raised. (On a gain-phase plot, the "loop" corresponding to the mode never crosses the $-180\text{-deg} \pm n * 360\text{-deg}$ line, even for zero damping.)

2) A gain stabilized mode is one which is closed-loop stable for the selected loop gain and assumed damping ratio, but can become unstable if the gain is raised or the damping ratio reduced. (On a gain-phase plot, the corresponding "loop" crosses the $-180\text{-deg} \pm n * 360\text{-deg}$ line if damping ratio is sufficiently small.)

A phase stabilized mode is clearly more desirable as its stability does not depend upon damping ratio, a parameter whose value is rarely known with any precision.

As can be seen in Fig. 8, modal coupling with the "rigid body" servo design (step 1) resulted in Mode 5 (15 Hz) becoming unstable. The flexible body compensation stage (Fig. 7) developed in step 2 is a phase notch selected with the objective of phase stabilizing Modes 5 and 11. It contributes ~72-deg phase lead at 15 Hz, thereby phase stabilizing Modes 4 and 5. Its rapid phase dropoff between 15 Hz and 40 Hz also permits simultaneous phase stabilization of Mode 11. Observe, in Fig. 9b, that no modes rely on gain stabilization, although the weak coupling of Modes 7 and 8 (as evidenced by the small "loops") could easily be reversed if the structural model were in error.

Parametric studies were conducted to determine sensitivity to modeling. Parameters varied included radial stiffness of the elevation bearing, mass and inertia of the PIA, c.m. location of PIA relative to gimbal axis, stiffness of the solar panel, and mass distribution on the solar panel. Although studies did not show instability under any conditions, they did show sufficient variation in modal properties to prompt the addition of an optional notch filter (ONF). The ONF consists of an extra stage in the compensation filter electronics, with a transfer function form similar to that of the flexible dynamic compensation stage in Fig. 7. The ONF stage is wired into the electronics unit, but is nominally bypassed. Provision was made to connect it easily at a later time (after tests) and components were procured to allow selection of a wide range of parameter values in the transfer function.

Even with the ONF there was concern that an unforeseen situation might be encountered downstream which could not be compensated with a single-stage notch. As a fallback position, a parallel, lower-bandwidth, compensation filter was included. Called SAD (secondary azimuth day), this new filter could be selected by ground command to the spacecraft and was designed to preclude any noticeable interaction between the servo loop and flexible dynamics. Pointing and raster performance requirements were waived for operation with the SAD filter, although an effort was made to come as close as possible, consistent with stability considerations.

V. Design Verification Using Ground Test Data

Test Objectives and Configurations

Because of the critical dependence of the despin control loop design on the sail and PIA flexible dynamics, a series of extensive ground tests of the despun structure were conducted with the basic objective of verifying the stability of the control system at the structural mode frequencies. Three test phases (summarized in Table 1) carried out over a 1½-yr time span, comprised the ground test program. These tests included initial testing of a mass model mockup of the structure (dubbed the T1 vehicle), flight structure testing, and a final structural response test using the full, flight configuration Solar Observatory.

A general functional block diagram of the Phase I and II test configurations is given in Fig. 10. For these tests, which involved determination of structural transfer functions prior to obtaining actual sensors, rotary accelerometers were mounted at the forward end of the PIA in place of the sun sensors. During open-loop tests, torque disturbances were applied individually at the two bearing assemblies by applying inputs (sinusoidal, impulse, step, or random) to the torque motors. The structural paths from controller to sensor, around which the servo loops are closed, were measured by direct observation of the rotary accelerometer outputs.

The open-loop structural transfer functions (gain and phase vs frequency) were obtained directly, using digitally generated random and chirp (i.e., fast sine sweep) inputs to the torque

Table 1 OSO structural response test summary

Test phase	Test configuration	Test objectives	Test results and impact on servo design
I. Mass model (T1) Test (May 1973)	Mockup of despun payload structure	Structure transmissibility for verification and update of analytical model	No major differences in azimuth response between analytical and mass model[a]
	Accelerometers mounted at sensor location	Structural damping measurements	Significant elevation structure coupling led to structural model modification, servo redesign, and structure modification
	No control electronics	Effect of air on structural damping	$0.18\% \leq \xi(\text{measured}) \leq 3\%$
	Primarily open-loop testing		No change in damping due to air test
			Inclusion of secondary azimuth day shaping
II. Flight structure test (June 1974)	Flight configuration despun payload	Flight structure transmissibility for control system interaction analysis	Verified adequacy of structural modifications resulting from T1 test
	Accelerometers mounted at sensor location	Closed-loop servo stability margin verification	Significant azimuth response differences between experiments in 20- to 70-Hz region; 90-Hz CNRS mode
	Simulated control system		Redesign of azimuth servo dynamics including backup loop
	Open and closed-loop testing		
III. Flight spacecraft test (Dec. 1974)	Full flight configuration observatory structure	Stability margin evaluation for flight vehicle	Structural coupling weaker
	No accelerometers		All modes gain stable
	Flight sensors and electronics		Minimal difference between experiments
	Closed-loop testing		

[a] One apparent difference was traced to errors in mockup model construction.

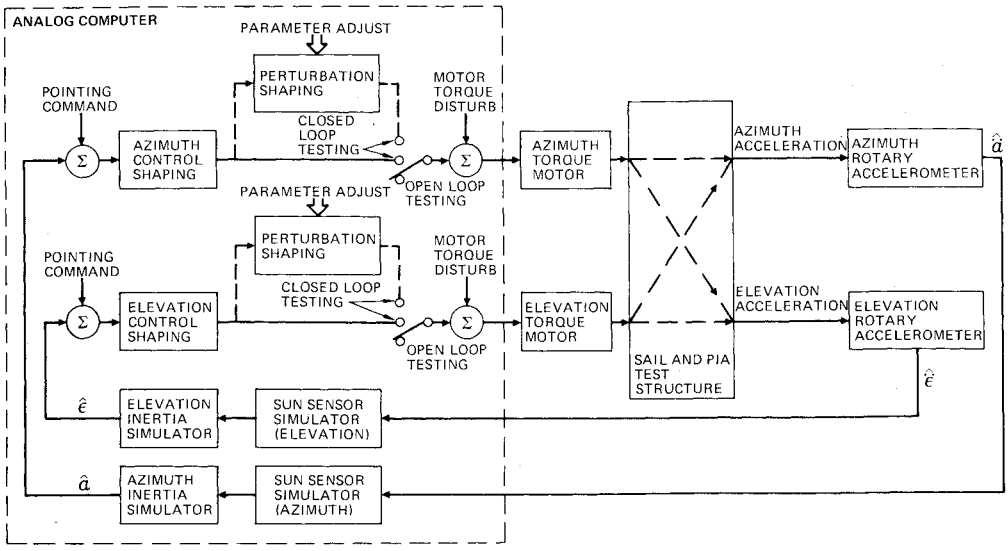

Fig. 10 OSO structural response test configuration (Phases I, II).

motor with digital Fourier analysis of the return accelerometer response. The resulting transfer function was calculated based on a time average of 40 repeated runs.

In order to observe actual closed-loop servo stability (or instability), closed-loop testing was incorporated into the test program. During initial closed-loop testing in Phase II, the outputs of the two accelerometers were shaped, using external electronics on an analog computer, to derive simulated sun sensor output pointing signals. The resulting control loop position error signals drove shaping networks, also simulated on the computer. These shaped error signals (now feedback torque commands) were used to drive the respective azimuth and elevation torque motors contained in the bearing assemblies. Thus, the closed-loop control system dynamic behavior could be observed when the servos were closed around actual payload structure.

For this phase of structural dynamics evaluation, closed-loop stability margin testing was used to analyze the strength of the structural interaction. By inserting various types of shaping filters in series with the error shaping (as is shown in Fig. 10) attempts were made (based on the analytical structural dynamics model) to induce control loop instabilities at isolated mode frequencies. The amount of shaping perturbation (gain and/or phase) required to cause a neutral stability condition defined the margin for that mode.

The last test phase involved using the flight spacecraft and incorporated the actual control electronics, sensors, and structure. For this final verification test, only closed-loop stability margin testing was used to analyze the strength of the structural interaction. Again, attempts were made (now using the previously measured control loop transfer function) to create instabilities in the individual control loops and determine actual system stability margins with the flight control system configuration.

Open-Loop Transfer Function Tests

The effect of the measured flexible dynamics of the sail and PIA on the control system was analyzed by convolving the impulse response function of an analytical model of the control loop with the measured structural response function. This is accomplished equivalently by multiplication of the structure and control system transfer functions defined in the frequency domain, i.e.,

$$G_{OL}(s) = \underbrace{[G_{\text{sensor}}(s) \times G_{\text{shaping}}(s)]}_{\text{analytical models}} \underbrace{\left[\frac{1}{Is^2}\right]}_{\substack{\text{rigid body}\\ \text{inertia}\\ \text{(analytical)}}} \times \underbrace{\left[\frac{I\ddot{\alpha}(s) \times G_{\text{motor}}(s)}{U_{\alpha(s)}}\right]}_{\substack{\text{measured transmissibility}\\ \text{data using torquers and}\\ \text{accelerometers}}}$$

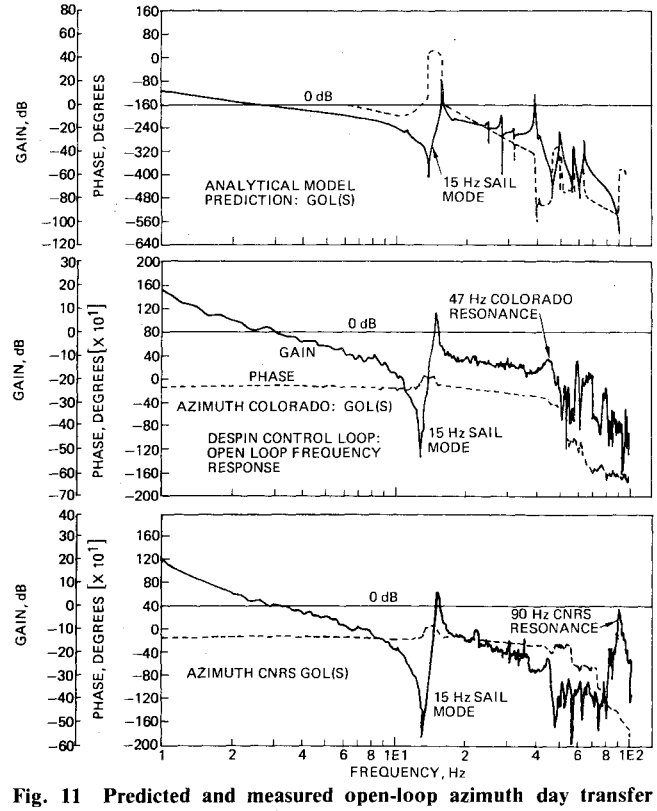

Fig. 11 Predicted and measured open-loop azimuth day transfer functions (final loop shaping).

Control system stability can then be evaluated using standard Bode and Nichols analysis techniques. The azimuth control loop transfer functions (Bode plots) developed during Phase II testing are shown in Fig. 11. The plots compare the characteristics of the analytical model dynamics (Fig. 11a) with the measured structure dynamics for the two payload experiments (Figs. 11b and 11c) with the final, flight shaping dynamics. The data show the 15-Hz sail torsional mode to be the most strongly coupled flexible mode with good agreement between theoretical and measured interaction. This mode is phase stabilized by the servo with modal stability independent of structural damping or coupling strength variations.

Significant differences observed in Phase II testing between the two experiments in the 30-60-Hz band and at 90 Hz resulted in reduced gain and phase margins as compared to predicted values. Consequently, the optional notch filter, which had been designed into the control electronics, was set

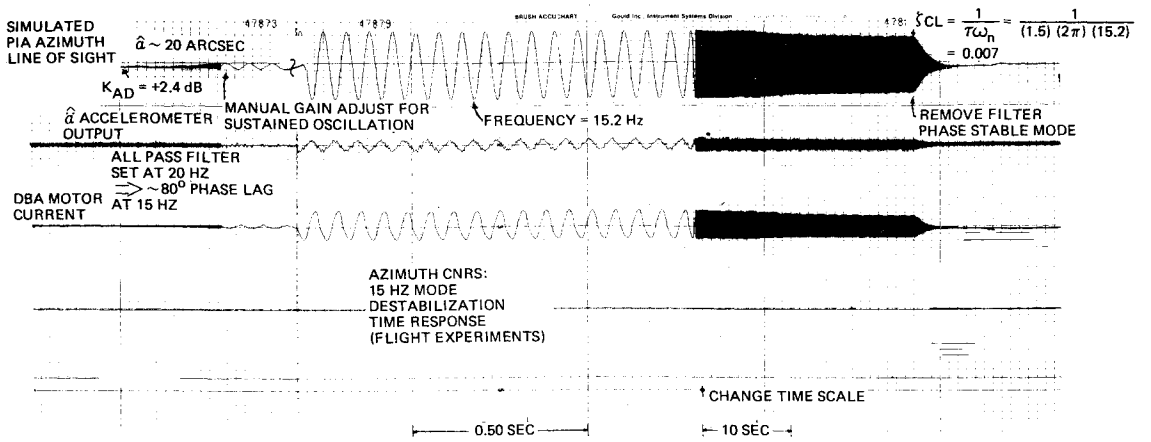

Fig. 12 15-Hz mode destabilization time response.

at 50 Hz and added to the control loop shaping. Minor adjustments were made to the basic shaping to maintain adequate phase margin at the 15-Hz modal frequency.

Closed-Loop Test Results

During Phase II and III testing, a second technique was used to evaluate the interaction between the control system and physical structural dynamics – stability margins of several of the strongly coupled modes were measured directly. The procedure used in this test was to insert perturbation filters (e.g., notch or "all-pass"), implemented on an analog computer, in series with the closed control loop. By manually adjusting the filter parameters, precise phase and/or gain perturbations could be introduced in desired frequency bands of the control loop transfer function. Predictions of system gain and phase stability margins (including effects of the measured structure characteristics) were obtained analytically. These stability margins were measured by adjusting perturbation filter parameters to reduce the margin to zero and observing that the system is indeed unstable at that frequency; that is, by slowly altering the loop transfer function at the modal frequencies of interest, the stability margins were reduced until the mode was made unstable as observed by system "buzzing." For the Phase II test, the simulated control loop dynamics were closed around the flight structure, as shown in Fig. 10. During full spacecraft testing (Phase III), the complete flight sail control system (sensor, control electronics, and motor) was used, giving the in-orbit system configuration. The full observatory test also included the use of the control system telemetry for an evaluation of the ability to diagnose an in-orbit instability from the available telemetry (sensor output, control loop error, and motor torque).

An example of this test technique is shown in the time history given in Fig. 12 in which the 15-Hz sail mode was destabilized. A phase shift filter $[G(s) = (s-\omega_0/s+\omega_0)]$ was set to reduce gradually the phase margin of the 15-Hz mode. In addition, the loop gain was manually increased until an oscillation was observed on the torque motor current. The gain and phase perturbation required to achieve instability defined the actual stability margin. For the example shown, the 15-Hz mode was demonstrated to be gain as well as phase stable – an effect not predicted by the measured system open-loop transfer function. Phase lag alone was unable to destabilize the mode. An additional, slight gain increase was required to induce instability. For the particular test case shown in Fig. 12, marginal stability occurred with a phase lag (at 15-Hz) of 80 deg and a gain perturbation of +2.5 dB. Thus, the mode coupling strength predicted by the loop transfer function is slightly overstated.

After sustained oscillation was achieved, the filter was switched out, allowing the mode oscillation to decay. This defined the composite closed-loop damping (structure plus servo) of the mode (0.7% for this mode).

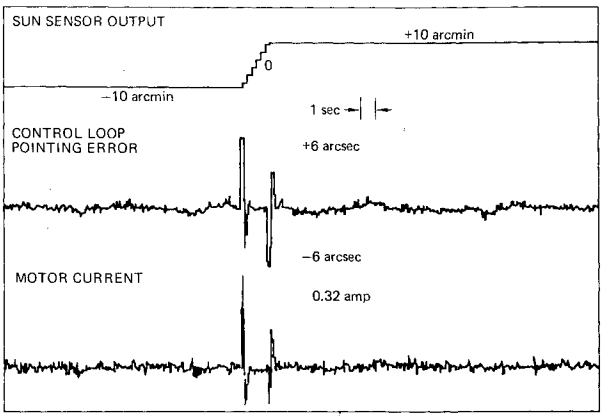

Fig. 13 OSO-8 control system telemetry during in-orbit maneuver.

These test data were used in conjunction with the earlier transfer function data to define the expected in-orbit stability margins of the system. Based on this tests, it was decided that sufficient margin existed and no additional design change or further testing was required.

VI. In-Orbit Response Characteristics

OSO-8 was launched successfully on June 21, 1975, by a Delta launch vehicle from the Eastern Test Range. Upon initial acquisition by the ground station, the sail control system was commanded into primary day control mode in which the sun sensors are used in the precision (wide bandwidth) sun tracking mode. The response of the azimuth control loop in this mode is shown in the time history of loop error and torque motor current telemetry (Fig. 13). The figure shows the control system response during a maneuver in which the experiment line-of-sight is slewed in azimuth ±10 arc min about the center of the solar disk. The normal response of the control system with only low-level background noise is indicative of the stability of the servo. This response can be compared to the results of the ground destabilization testing discussed previously. The entire control system has been exercised in all control modes, including high scan rate rasters and long-term sun tracking with no conditions of either instability or marginal stability observed.

VII. Concluding Remarks

It is appropriate at this point to put in perspective the various analyses, simulation, and tests surrounding the azimuth day servo loop design for OSO-8. First, it should be noted that, although attention in this paper has been focused on the azimuth day servo loop, this loop is only one of seven servo loops necessary for attitude control of the PIA experiment package. The azimuth day control loop was chosen

as the subject of this paper as it experienced the most design problems, particularly with respect to flexible dynamics interactions.

The existence of a flexible dynamics problem was recognized at the outset of the program, although not fully appreciated until examined in greater depth. Flexible body compensation in the form of a phase notch for the 15-Hz mode was incorporated during the proposal. Also, the large resonances at ~45 Hz and at ~60 Hz were predicted in model analyses at that time, although several of the nearby, less-pronounced modes were not as accurately predicted. The 90-Hz resonance of the CNRS experiment and the ~13 dB additional gain of the Colorado transfer function were not predicted by any of the analytical models. The uncertainties associated with the flexible dynamics model became evident as a result of parameter studies conducted near the start of the program. These uncertainties prompted several actions: 1) The addition of the optional notch filter (with its parameter selection left open); 2) the addition of the initial secondary azimuth day loop as an out of spec, but definitely stable backup; and 3) the planning of the T1 test with an objective of providing verification of the flexible dynamics model as early as possible and in time to make modifications, if required. Results of the T1 test provided valuable data on structural damping (generally there was less damping than expected) and verified many aspects of the analytical model, including the 15-Hz mode which had been electrically compensated. Some discrepancies in the azimuth loop transfer function between T1 test and analytical predictions also occurred, but these were traced to deficiencies in the mockup structure for the PIA experiments. The azimuth loop compensation was not changed as a result of the T1 test.

Due to the structural changes following the T1 test and the fact that the T1 mockup structure had been inadequate in some ways, there was sufficient uncertainty that the F1 transmissibility test, which up to that time had been only tentative, became a necessity. The F1 tests, which included flight quality experiment packages, provided some new surprises. Heading the list were the truly large 90-Hz resonance due to the CNRS experiment and the 13-dB gain difference at high frequencies between the CNRS and Colorado transfer functions. The analytical model as well as T1 test results had indicated essentially identical transfer functions for the two sensor outputs. These discrepancies led to changes in the azimuth compensation. Not only was the optional notch filter selected to gain stabilize modes around 50 Hz, but the 15-Hz phase notch was intensified to provide the necessary phase lead for stability. The bandwidth of one secondary azimuth day loop (there are two redundant control electronics) was increased somewhat to provide performance closer to the desired specification, since the likelihood of its eventual use was increased. Thus, there were six orbit day azimuth control options developed (3 control loops × 2 sensor configurations).

The final test phase incorporating all flight control system elements with the complete flight structure yielded additional, although less startling, differences with the earlier tests. The dramatic difference between the azimuth response of the two experiments was not observed when the sensors were used in place of accelerometers. All modes were verified to be gain stabilized with stability margins above 30 Hz exceeding 30 dB, which was higher than those previously predicted. No additional modifications were made or tests performed.

In-orbit experience with the spacecraft tends to validate the results of the final test phase with no significant coupling or marginal stability conditions observed during two years of flight operation. The backup control loops have never been exercised, and measured pointing stability exceeds the original requirement by 2:1.

The experience gained on the OSO project has been carried over by the authors to other programs. The analysis methods have grown into a general purpose computer program which has been applied on several projects and is still undergoing continued improvements. Likewise, the test method employing loop shaping perturbation has found application on other programs as a convenient low cost, reliable means to measure control loop stability margins.

References

[1] Bodley, C.S., Devers, A.D., and Park, A.C., "Computer Program System for Dynamic Simulation and Stability Analysis of Passive and Actively Control Spacecraft," Martin Marietta Rept. MCR-75-17, NASA Contract NAS5-11996, April 1975.

[2] Aubrun, J.N., Bushnell, D., Ho, J.Y.L., and Margulies, G., "Multibody Flexible Spacecraft Integrated Analysis: Structures, Dynamics, Control," *Symposium on Dynamics and Control of Large Flexible Spacecraft,* Blacksburg, Va., June 1977.

[3] Likins, P.W., "Analytical Dynamics and Non-Rigid Spacecraft Simulation," Jet Propulsion Laboratory, Pasadena, Calif., JPL TR32-1593, July 15, 1974.

[4] Likins, P.W., "Dynamics and Control of Flexible Space Vehicles," Jet Propulsion Laboratory, Pasadena, Calif., TR32-1329,Revision 1, Jan. 15, 1970.